

# Color-Singlet $\psi_Q$ Production at $e^+e^-$ Colliders

Peter Cho and Adam K. Leibovich

*Lauritsen Laboratory*

*California Institute of Technology*

*Pasadena, CA 91125*

(September 14, 2018)

## Abstract

We calculate in closed form the complete  $\mathcal{O}(\alpha_s^2)$  color-singlet differential cross section for  $e^+e^- \rightarrow \gamma^* \rightarrow \psi_Q + X$  scattering. The cross section reduces at high energies to a heavy quark fragmentation form. We find that the energy scale at which the approximate fragmentation result becomes reliable exceeds the  $\psi_Q$  mass by more than an order of magnitude. We also discuss the color-singlet model's predictions for direct  $J/\psi$  angular and energy distributions at CLEO.

## I. INTRODUCTION

During the past few years, there has been renewed interest in the study of heavy quarkonium systems. Much of the recent work on this subject has been stimulated by large discrepancies between old predictions and new observations of Psi and Upsilon production at several experimental facilities. Orders of magnitude disagreements between theory and data have seriously undermined the conventional “color-singlet model” (CSM) picture of quarkonia formation [1–5]. In this model, charmonia and bottomonia mesons are presumed to exclusively originate from short distance processes that create heavy quark-antiquark pairs in colorless configurations. The quantum numbers of pairs produced in high energy collisions on time scales short compared to  $\Lambda_{QCD}$  are required to precisely match those of the final state hadrons into which they nonperturbatively evolve. Although this CSM picture is simple, it does not explain several gross features of recent charmonia and bottomonia data collected at the Fermilab Tevatron [6–8]. It consequently must be abandoned as a complete theory.

A new framework for treating quarkonia systems called Nonrelativistic Quantum Chromodynamics (NRQCD) has been developed within the past few years [9]. This effective field theory generalizes and improves upon the CSM in several regards. It allows for short distance processes to create heavy quark-antiquark pairs in color-octet configurations which can hadronize over much longer length scales into colorless final state quarkonia. Calculations which include this color-octet mechanism appear to successfully describe Tevatron measurements [10–13]. But in order to establish the validity of this new paradigm, it is necessary to consider quarkonia production in other experimental situations.

Braaten and Chen have suggested that a clean signature of the color-octet mechanism may be observable in  $\psi_Q$  production at electron-positron colliders [14]. These authors have noted that the angular distribution of colored  $Q\bar{Q}$  pairs near the endpoint region may qualitatively differ from that of their colorless counterparts. If this effect could be observed, it would support the color-octet production picture. It might also permit an independent

determination of the numerical values for certain NRQCD matrix elements.

Before the search for color-octet quarkonia production in  $e^+e^-$  annihilation can begin, one must first know the precise CSM prediction. Within the NRQCD framework, the color-singlet cross section is also expected to be quite accurate for all energies except near the endpoint region [14]. In this note, we therefore build upon previous studies reported in the literature [15–18] and calculate the complete  $\mathcal{O}(\alpha_s^2)$  color-singlet cross section for  $e^+e^- \rightarrow \psi_Q + X$  scattering. We examine the contribution to  $\psi_Q$  production from the short distance modes  $e^+e^- \rightarrow Q\bar{Q}[{}^3S_1^{(1)}] + g + g$  and  $e^+e^- \rightarrow Q\bar{Q}[{}^3S_1^{(1)}] + Q + \bar{Q}$ ,<sup>1</sup> and we derive a closed form expression for the differential cross section. We then discuss the implications of the CSM result for direct  $J/\psi$  observations at CLEO. Finally, we compare heavy quark fragmentation predictions with the color-singlet cross section and determine the energy scale at which fragmentation approximations become reliable.

## II. INCLUSIVE ANGULAR DISTRIBUTIONS IN ELECTRON-POSITRON COLLISIONS

It is useful to note some general features of inclusive, unpolarized  $\psi_Q$  production in  $e^+e^-$  annihilation. Unitarity, parity and angular momentum considerations restrict the form of the differential cross section expression

$$\frac{d^2\sigma}{dE_3 d\cos\theta_3} \left( e^+(p_1)e^-(p_2) \rightarrow \gamma^* \rightarrow \psi_Q(p_3) + X \right) = S(E_3) \left[ 1 + \alpha(E_3) \cos^2\theta_3 \right]. \quad (2.1)$$

In particular, the allowed range for the angular coefficient function is constrained to lie within the interval  $-1 \leq \alpha(E_3) \leq 1$ . We sketch a derivation of this result below.

It is instructive to consider the subprocess  $\gamma^*(P) \rightarrow \psi_Q(p_3) + X(P - p_3)$  where the intermediate photon is either longitudinally or transversely aligned. The squared amplitude for this decay

---

<sup>1</sup>We indicate the angular momentum and color-singlet quantum numbers of the  $Q\bar{Q}$  pair which hadronizes into the final state  $\psi_Q$  meson inside square brackets.

$$|\mathcal{A}|^2 = \sum_{\lambda} \varepsilon_{\mu}(P; \lambda) \varepsilon_{\nu}(P; \lambda)^* F^{\mu\nu} \quad (2.2)$$

involves a form factor  $F^{\mu\nu}$  which can be decomposed in terms of tensors that respect parity and gauge invariance:

$$F^{\mu\nu} = -F_1 \left( g^{\mu\nu} - \frac{P^{\mu} P^{\nu}}{P^2} \right) + \frac{F_2}{P^2} \left( p_3^{\mu} - \frac{P \cdot p_3}{P^2} P^{\mu} \right) \left( p_3^{\nu} - \frac{P \cdot p_3}{P^2} P^{\nu} \right). \quad (2.3)$$

Working in the  $\gamma^*$  rest frame where the  $\psi_Q$  four-momentum looks like  $p_3 = (E_3, \vec{p}_3) = (E_3, |\vec{p}_3| \sin \theta \cos \phi, |\vec{p}_3| \sin \theta \sin \phi, |\vec{p}_3| \cos \theta)$ , we find that the squared decay amplitude for a longitudinally polarized virtual photon reduces to

$$|\mathcal{A}|_L^2 = F_1 [1 + \alpha_L \cos^2 \theta], \quad (2.4a)$$

with

$$\alpha_L = \frac{|\vec{p}_3|^2}{P^2} \frac{F_2}{F_1}. \quad (2.4b)$$

For a transverse  $\gamma^*$ , the squared amplitude takes the form

$$|\mathcal{A}|_T^2 = \left( 2F_1 + \frac{|\vec{p}_3|^2}{P^2} F_2 \right) [1 + \alpha_T \cos^2 \theta], \quad (2.5a)$$

where

$$\alpha_T = -\frac{|\vec{p}_3|^2 F_2}{2P^2 F_1 + |\vec{p}_3|^2 F_2} = -\frac{\alpha_L}{2 + \alpha_L}. \quad (2.5b)$$

Since both  $|\mathcal{A}|_L^2$  and  $|\mathcal{A}|_T^2$  are nonnegative, eqs. (2.4) and (2.5) imply  $\alpha_L \geq -1$  and  $-1 \leq \alpha_T \leq 1$ .

Helicity conservation requires the intermediate photon in  $e^+e^- \rightarrow \gamma^* \rightarrow \psi_Q + X$  to be transversely aligned relative to the beam axis in the  $m_e = 0$  limit. The  $\psi_Q$  meson's angular distribution is therefore significantly restricted by simple symmetry considerations. In fact, the inclusive angular distribution of *any* unpolarized particle which is produced in electron-positron colliders operating well below the  $Z$ -pole goes as  $1 + \alpha_T \cos^2 \theta$  with  $-1 \leq \alpha_T \leq 1$ . So while observation of a pure  $\sin^2 \theta$  distribution for a lepton or hadron at a collider like CLEO is possible, a pure  $\cos^2 \theta$  distribution is not. As we shall see, all color-singlet  $\psi_Q$  predictions are consistent with these general considerations.

### III. COLOR-SINGLET $\psi_Q$ PRODUCTION

The simplest parton level process which mediates color-singlet production of  $J^{PC} = 1^{--}$  quarkonia is given by  $e^+e^- \rightarrow Q\bar{Q}[^3S_1^{(1)}] + g + g$ . Color, parity and charge conjugation conservation require two gluons to appear in the final state along with the colorless  $Q\bar{Q}[^3S_1^{(1)}]$  pair. This channel consequently contributes to the  $\psi_Q$  cross section starting at  $\mathcal{O}(\alpha_s^2)$ . Color singlet production also proceeds at the same order in perturbative QCD through the mode  $e^+e^- \rightarrow Q\bar{Q}[^3S_1^{(1)}] + Q + \bar{Q}$ . These two distinct reactions have been considered separately in the literature [15–18]. We will reexamine their joint impact upon Psi and Upsilon production and derive a closed form analytic expression for  $d^2\sigma/dE_3 d\cos\theta_3$ . We can then compare the relative magnitudes of the gluon and quark processes as a function of center-of-mass energy  $\sqrt{S}$ .

The leading order diagrams which mediate  $e^+(p_1)e^-(p_2) \rightarrow Q\bar{Q}[^3S_1^{(1)}](p_3) + g(p_4) + g(p_5)$  and  $e^+(p_1)e^-(p_2) \rightarrow Q\bar{Q}[^3S_1^{(1)}](p_3) + Q(p_4) + \bar{Q}(p_5)$  scattering are illustrated in Figs. 1 and 2. The hard collisions pictured in the figures form on short time scales a heavy quark and antiquark which fly out from the primary interaction point in nearly parallel directions and almost on-shell. The  $Q\bar{Q}$  pair then evolves over a much longer time interval into a physical  $\psi_Q$  bound state. Working within the NRQCD framework and using computational methods discussed in Refs. [4,12,13], one can straightforwardly calculate the amplitudes for these processes. Their squares factorize into products of short distance coefficient functions and long distance NRQCD matrix elements.

Integrating the squared amplitudes over the three particle phase space factor

$$d\Phi_3 = (2\pi)^4 \delta^4(p_1 + p_2 - p_3 - p_4 - p_5) \prod_{i=3}^5 \frac{d^3p_i}{(2\pi)^3 2E_i} \quad (3.1)$$

is somewhat involved. As a simplifying measure, we rescale all dimensionful quantities relative to the beam energy  $E$  and work with the dimensionless variables  $z_i = E_i/E$ ,  $\vec{q}_i = \vec{p}_i/E$ ,  $x_i = \cos\theta_i$  and  $\delta = 2M_Q/E$ . The phase space factor for the reaction with gluons in the final state can then be reduced to the form

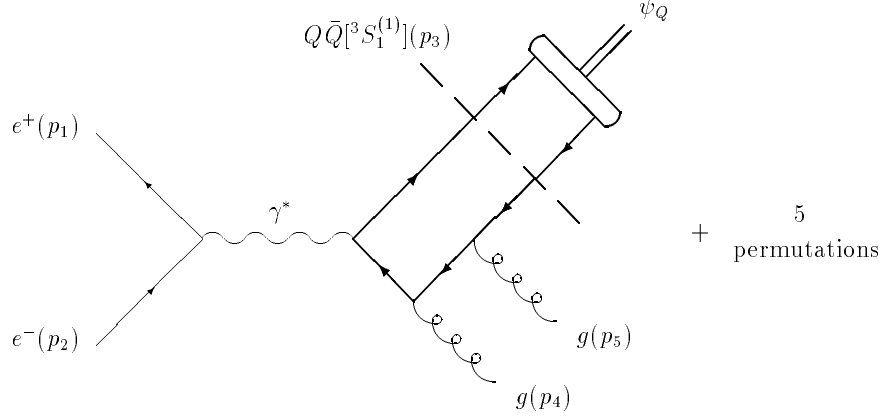


FIG. 1. Leading order Feynman graphs which mediate  $e^+e^- \rightarrow \gamma^* \rightarrow Q\bar{Q}[{}^3S_1^{(1)}] + g + g \rightarrow \psi_Q + X$  scattering.

$$d\Phi_3 = \frac{(2\pi)^{-4}}{8} E^2 \frac{dz_3 dx_3 dz_- dw}{\sqrt{(1-K^2)(1-x_3^2) - w^2}} \quad (3.2)$$

where

$$z_- = z_4 - z_5 \quad (3.3a)$$

$$|\vec{q}_-| = \sqrt{4 - 4z_3 + \delta^2 + z_-^2} \quad (3.3b)$$

$$|\vec{q}_3| = \sqrt{z_3^2 - \delta^2} \quad (3.3c)$$

$$K = \frac{z_-(2 - z_3)}{|\vec{q}_-||\vec{q}_3|} \quad (3.3d)$$

$$w = x_- + Kx_3. \quad (3.3e)$$

The same result holds for the quark process with the simple alteration  $|\vec{q}_-| = \sqrt{4 - 4z_3 + z_-^2}$ .

The available phase space volume clearly depends upon the masses of the final state bodies. For the  $e^+e^- \rightarrow Q\bar{Q}[{}^3S_1^{(1)}] + g + g$  channel, the limits of integration for the remaining energy and angular variables in eq. (3.2) are given by

$$\delta \leq z_3 \leq 1 + \frac{\delta^2}{4} \quad (3.4a)$$

$$-1 \leq x_3 \leq 1 \quad (3.4b)$$

$$-\sqrt{z_3^2 - \delta^2} \leq z_- \leq \sqrt{z_3^2 - \delta^2} \quad (3.4c)$$

$$-\sqrt{(1-K^2)(1-x_3^2)} \leq w \leq \sqrt{(1-K^2)(1-x_3^2)}. \quad (3.4d)$$

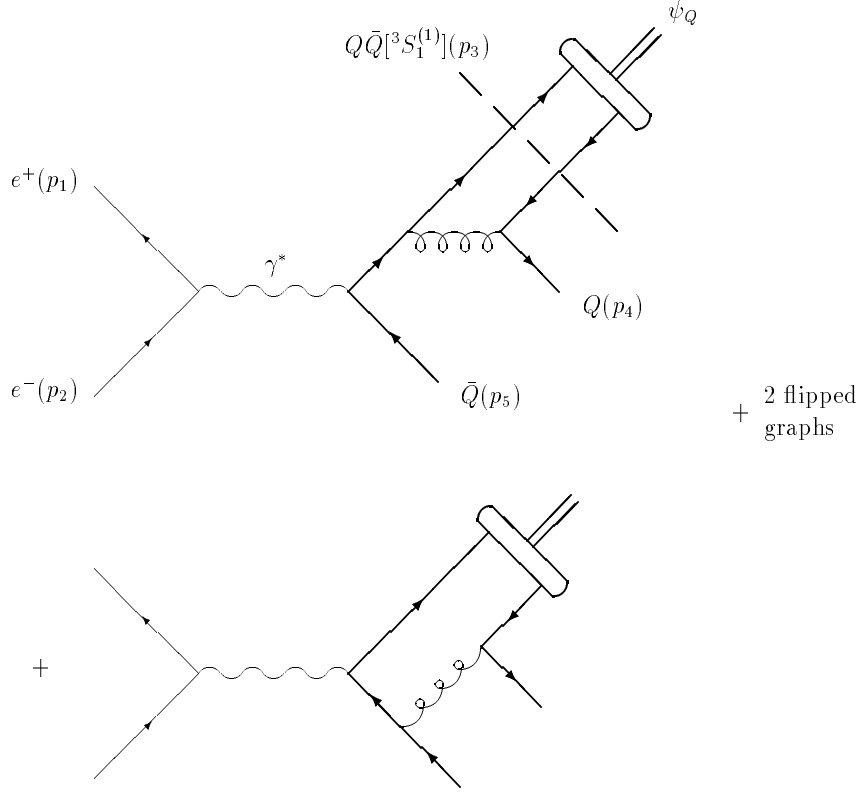


FIG. 2. Leading order Feynman graphs which mediate  $e^+e^- \rightarrow \gamma^* \rightarrow Q\bar{Q}[{}^3S_1^{(1)}] + Q + \bar{Q} \rightarrow \psi_Q + X$  scattering.

The corresponding limits for the  $e^+e^- \rightarrow Q\bar{Q}[{}^3S_1^{(1)}] + Q + \bar{Q}$  mode

$$\delta \leq z_3 \leq 1 \quad (3.5a)$$

$$-1 \leq x_3 \leq 1 \quad (3.5b)$$

$$-\sqrt{\frac{(4-4z_3)(z_3^2-\delta^2)}{4-4z_3+\delta^2}} \leq z_- \leq \sqrt{\frac{(4-4z_3)(z_3^2-\delta^2)}{4-4z_3+\delta^2}} \quad (3.5c)$$

$$-\sqrt{(1-K^2)(1-x_3^2)} \leq w \leq \sqrt{(1-K^2)(1-x_3^2)} \quad (3.5d)$$

are more tight due to the additional heavy quark and antiquark in the final state.

After inserting the averaged squared amplitudes and reduced phase space factors into the formula

$$d\sigma = \frac{1}{8E^2} \overline{\sum} |\mathcal{A}|^2 d\Phi_3, \quad (3.6)$$

we can analytically integrate over  $w$  and  $z_-$  and obtain differential expressions of the form (2.1). We display the resulting  $S(z_3)$  and  $\alpha(z_3)$  functions for the  $e^+e^- \rightarrow Q\bar{Q}[{}^3S_1^{(1)}] + g + g$

and  $e^+e^- \rightarrow Q\bar{Q}[{}^3S_1^{(1)}] + Q + \bar{Q}$  processes in the appendix. As a check, one can verify that  $|\alpha_{\text{gluon}}|$  and  $|\alpha_{\text{quark}}|$  do not exceed unity within their allowed  $z_3$  ranges as required by the general constraints discussed in section II. The total  $\mathcal{O}(\alpha_s^2)$  angular coefficient function

$$\alpha_{\text{total}} = \frac{S_{\text{gluon}} \alpha_{\text{gluon}} + S_{\text{quark}} \alpha_{\text{quark}}}{S_{\text{gluon}} + S_{\text{quark}}} \quad (3.7)$$

also respects the bound  $-1 \leq \alpha_{\text{total}} \leq 1$ .

Another important check can be performed by considering the high energy behavior of the  $S(z_3)$  and  $\alpha(z_3)$  functions. In the  $z_3 \gg \delta$  limit, the color-singlet cross section reduces to

$$\begin{aligned} \frac{d^2\sigma}{dz_3 d\cos\theta_3}(e^+e^- \rightarrow \psi_Q + X) &= \frac{4\pi}{243} \frac{(\alpha_s \alpha_{EM} \mathcal{Q}_Q)^2}{m_Q^3 E^2} \langle 0 | \mathcal{O}_1^{\psi_Q}({}^3S_1) | 0 \rangle [1 + \cos^2\theta_3] \\ &\times \frac{z_3(1-z_3)^2(16 - 32z_3 + 72z_3^2 - 32z_3^3 + 5z_3^4)}{(2-z_3)^6}. \end{aligned} \quad (3.8)$$

After integrating over  $\cos\theta_3$  and recalling the relation  $\langle 0 | \mathcal{O}_1^{\psi_Q}({}^3S_1) | 0 \rangle = 9|\mathcal{R}(0)|^2/2\pi$  between the color-singlet NRQCD matrix element and the  $\psi_Q$  wavefunction at the origin [9], we can write the  $\psi_Q$  energy distribution as

$$\frac{d\sigma}{dz_3}(e^+e^- \rightarrow \psi_Q + X) = 2\sigma(e^+e^- \rightarrow Q\bar{Q}) \times \mathcal{D}_{Q \rightarrow \psi_Q}(z_3) \quad (3.9)$$

where  $\mathcal{D}_{Q \rightarrow \psi_Q}(z_3)$  denotes the heavy quark fragmentation function calculated in Ref. [19]. The complete  $\mathcal{O}(\alpha_s^2)$  color-singlet cross section thus correctly reproduces known fragmentation results at high energies.

#### IV. DIRECT $J/\psi$ PRODUCTION AT CLEO

$J/\psi$  production is currently under study at CLEO [20,21]. Charmonia observed at this  $e^+e^-$  facility mainly come from  $B$  meson decays. However, a clean sample of  $\psi$ 's originating from continuum production can be obtained by imposing a lower momentum cut on their dilepton decay products. Various characteristics of the resulting direct  $J/\psi$  data sample can then be compared with predictions based upon color-singlet and color-octet production mechanisms. Such experimental investigations are underway [22].

The angular distribution of direct  $J/\psi$  mesons represents one observable which can be measured at CLEO. In Fig. 3, we plot the CSM prediction for the angular coefficient function  $\alpha$ . The results displayed in the figure are based upon the input parameter values  $E = 5.29$  GeV,  $m_c = 1.48$  GeV,  $\alpha_s(2m_c) = 0.28$ ,  $\alpha_{EM}(2m_c) = 0.0075$ ,  $\mathcal{Q}_c = 2/3$  and  $\langle 0|\mathcal{O}_1^{J/\psi}(^3S_1)|0\rangle = 1.2$  GeV<sup>3</sup>. The dashed curve illustrates the function  $\alpha_{\text{gluon}}$  associated with  $e^+e^- \rightarrow c\bar{c}[^3S_1^{(1)}] + g + g$  scattering. The shape of this curve agrees with numerical

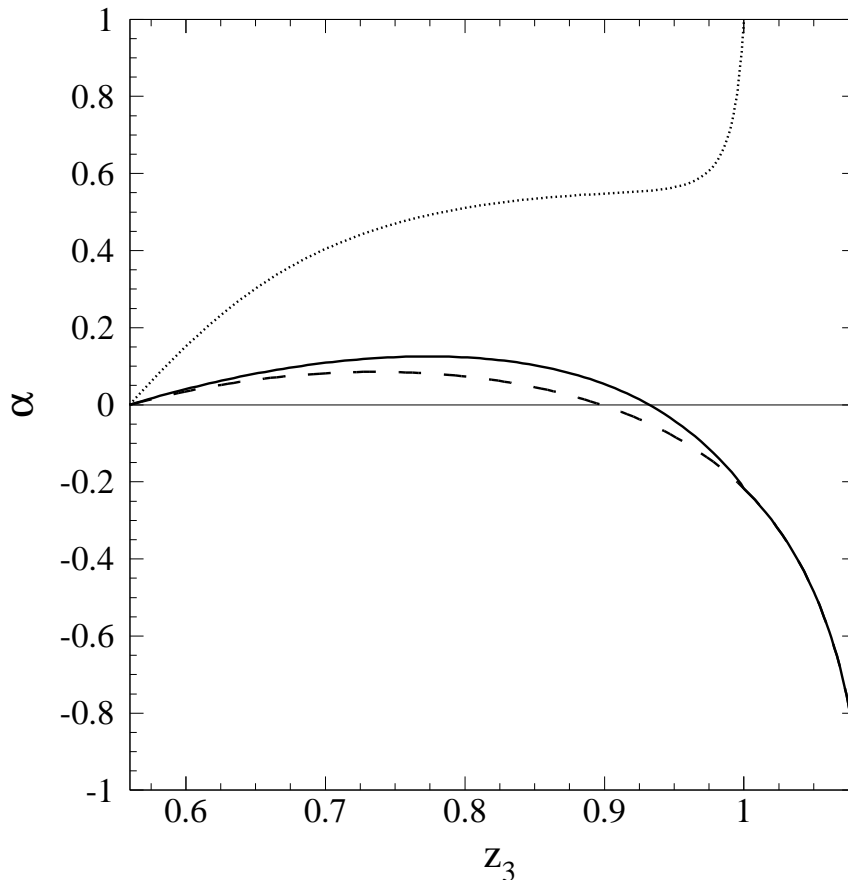


FIG. 3. Angular coefficient functions  $\alpha_{\text{gluon}}$  (dashed line),  $\alpha_{\text{quark}}$  (dotted line) and  $\alpha_{\text{total}}$  (solid line) plotted against dimensionless energy variable  $z_3$ .

results of Driesen *et al.* reported in Ref. [17]. The dotted line in Fig. 3 depicts the function  $\alpha_{\text{quark}}$  originating from the  $e^+e^- \rightarrow c\bar{c}[^3S_1^{(1)}] + c + \bar{c}$  mode. The shape of  $\alpha_{\text{quark}}$  is clearly quite different than that of  $\alpha_{\text{gluon}}$ . But since  $S_{\text{quark}}$  is substantially smaller than  $S_{\text{gluon}}$  at CLEO energies, it has only a small impact upon the total color-singlet function  $\alpha_{\text{total}}$  which is represented by the solid curve in Fig. 3. It is important to note that  $\alpha_{\text{total}}$  is predicted within

the CSM to be negative at the largest allowed values for  $z_3$ . On the other hand, color-octet effects may render  $\alpha_{\text{total}}$  positive in the endpoint region [14]. The angular distribution of the most energetic  $J/\psi$ 's at CLEO can therefore provide a valuable test of the color-octet mechanism.

The energy distribution of direct  $J/\psi$ 's is another quantity which can be used to probe theories of quarkonia production. In Fig. 4, we display the separate contributions to  $d\sigma/dz_3$  from the  $e^+e^- \rightarrow c\bar{c}[{}^3S_1^{(1)}] + g + g$  and  $e^+e^- \rightarrow c\bar{c}[{}^3S_1^{(1)}] + c + \bar{c}$  channels along with the total CSM prediction. The sensitivity of this energy observable to the charm mode is more

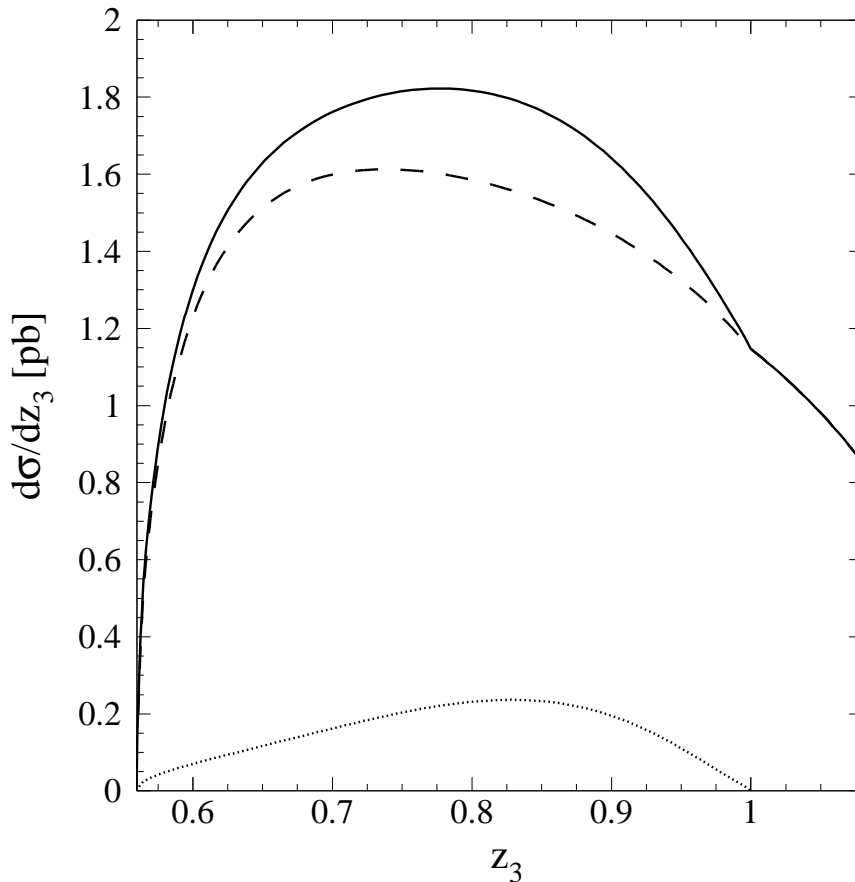


FIG. 4. Contributions to  $d\sigma/dz_3$  from the gluon (dashed line) and quark (dotted line) modes plotted against  $z_3$ . The CSM prediction for the total direct  $J/\psi$  energy distribution is represented by the solid curve.

pronounced than that of the angular coefficient function. The areas underneath the dashed, dotted and solid curves respectively equal 0.74 pb, 0.07 pb and 0.81 pb. The quark process

thus contributes at the 10% level to direct  $J/\psi$  production at CLEO.

The  $e^+e^- \rightarrow c\bar{c}[{}^3S_1^{(1)}] + c + \bar{c}$  mode is significantly phase space suppressed compared to  $e^+e^- \rightarrow c\bar{c}[{}^3S_1^{(1)}] + g + g$  at CLEO energies. As a result, its impact upon charmonia observables is minor. However, it is interesting to examine the relative importance of these two color-singlet channels as a function of center-of-mass energy. We plot in Fig. 5 the modes' separate contributions to the integrated  $J/\psi$  cross section along with their sum versus  $\sqrt{S} = 2E$ . We also display the integral of the charm quark fragmentation approximation (3.8). At low energies, the charm quark mode is negligible compared to its gluon counterpart. At larger

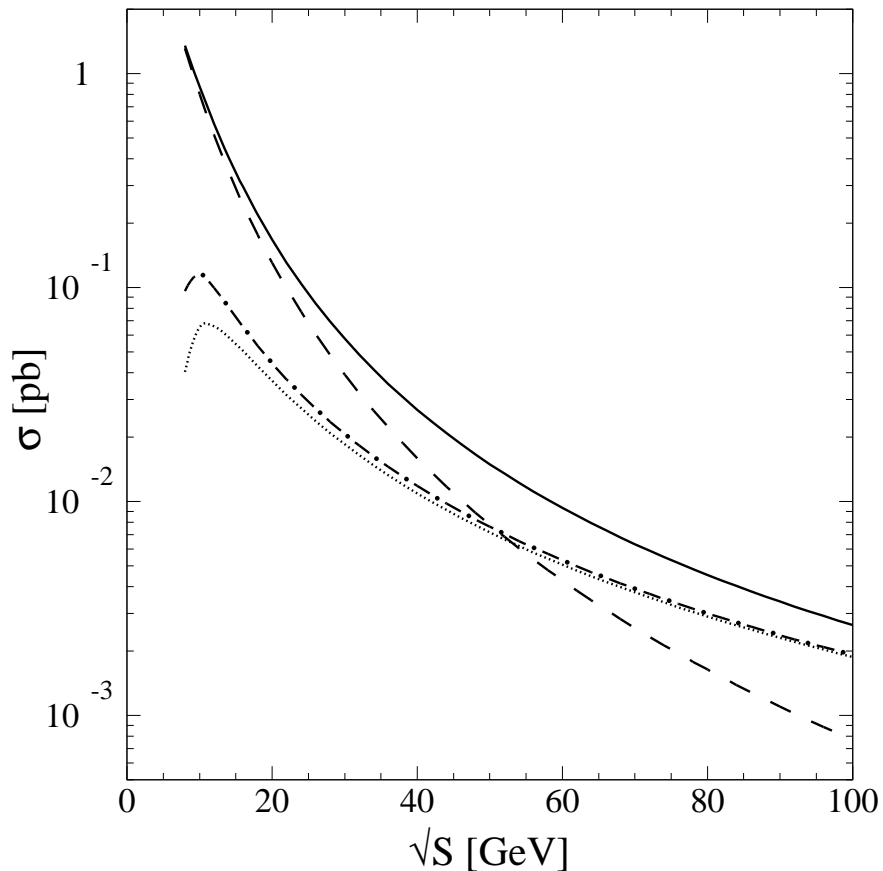


FIG. 5. Integrated cross sections for the gluon (dashed line) and charm quark (dotted line) modes plotted as a function of  $\sqrt{S}$ . The sum of the two is shown by the solid curve. The approximate charm quark fragmentation cross section is depicted by the dot-dashed curve.

values of  $\sqrt{S}$ , it becomes relatively more important. Finally, in the charm fragmentation limit  $\sqrt{S} \gg m_c$ , the quark mode dominates.

As can be seen in Fig. 5, the charm quark fragmentation curve rapidly asymptotes to the  $e^+e^- \rightarrow c\bar{c}[{}^3S_1^{(1)}] + c + \bar{c}$  cross section. But it is important to note that the crossover point at which the rates for the charm and gluon modes become equal occurs around  $\sqrt{S} \simeq 50$  GeV. Consequently, the fragmentation approximation does *not* accurately reflect the total color-singlet cross section until  $\sqrt{S}$  exceeds  $2m_c$  by more than an order of magnitude. This result for  $J/\psi$  production at lepton colliders is quite different than that for hadron accelerators. Previous investigations have found that fragmentation approximations are reasonably trustworthy for production of  $\psi$ 's at the Tevatron with  $p_\perp \gtrsim 10$  GeV [12,13]. The moral we thus draw from this study of charmonia at CLEO is that the validity of fragmentation predictions must be carefully checked on a case-by-case basis.

#### ACKNOWLEDGMENTS

We thank David Politzer for helpful discussions. The work of P.C. was supported in part by a DuBridge Fellowship and by the Department of Energy under Grant No. DE-FG03-92-ER40701. The work of A.L. was supported in part by the DOE under Grant No. DE-FG03-92-ER40701.

## APPENDIX:

We list here the color-singlet functions  $S$  and  $\alpha$  which enter into the differential cross section (2.1) at leading order in both the perturbative QCD and NRQCD velocity expansions. The contributions from the  $e^+e^- \rightarrow Q\bar{Q}[^3S_1^{(1)}] + g + g$  and  $e^+e^- \rightarrow Q\bar{Q}[^3S_1^{(1)}] + Q + \bar{Q}$  channels are separately displayed.

$e^+e^- \rightarrow Q\bar{Q}[^3S_1^{(1)}] + g + g$  mode:

$$\begin{aligned}
S_{\text{gluon}} &= \frac{\pi}{216} \frac{(\alpha_s \alpha_{EM} \mathcal{Q}_Q)^2}{\delta E^5} \frac{\langle 0 | \mathcal{O}_1^{\psi_Q} (^3S_1) | 0 \rangle}{(z_3 - 2)^2 (2z_3 - \delta^2)^3 (z_3^2 - \delta^2)} \\
&\times \left\{ 4 \left[ -\delta^2(4 + \delta^2)(48 + 48\delta^2 + 13\delta^4) + 32\delta^2(4 + \delta^2)(4 + 3\delta^2)z_3 \right. \right. \\
&\quad + 8(32 - 56\delta^2 - 24\delta^4 + \delta^6)z_3^2 - 16(32 + 4\delta^2 + 3\delta^4)z_3^3 \\
&\quad + 112(4 + \delta^2)z_3^4 - 128z_3^5 \left. \right] (2z_3 - \delta^2) \sqrt{z_3^2 - \delta^2} \\
&\quad + \left[ \delta^4(4 - \delta^2)(48 + 96\delta^2 + 13\delta^4) - 32\delta^4(28 - 3\delta^2 - 3\delta^4)z_3 \right. \\
&\quad + 8\delta^2(16 - 40\delta^2 - 27\delta^4 + \delta^6)z_3^2 + 16\delta^2(56 + 14\delta^2 - 3\delta^4)z_3^3 \\
&\quad \left. \left. - 16(4 - \delta^2)(4 + 5\delta^2)z_3^4 \right] (4z_3 - 4 - \delta^2) \ln \frac{2z_3 - \delta^2 + 2\sqrt{z_3^2 - \delta^2}}{2z_3 - \delta^2 - 2\sqrt{z_3^2 - \delta^2}} \right\} \tag{A1a}
\end{aligned}$$

$$\begin{aligned}
\alpha_{\text{gluon}}(z_3) &= \frac{\pi}{216} \frac{(\alpha_s \alpha_{EM} \mathcal{Q}_Q)^2}{\delta E^5} \frac{\langle 0 | \mathcal{O}_1^{\psi_Q} (^3S_1) | 0 \rangle}{(z_3 - 2)^2 (2z_3 - \delta^2)^3 (z_3^2 - \delta^2)} \\
&\times \left\{ 4 \left[ \delta^2(64 + 80\delta^2 + 76\delta^4 + 7\delta^6) - 96\delta^4(4 + \delta^2)z_3 \right. \right. \\
&\quad - 8(32 - 40\delta^2 - 44\delta^4 - \delta^6)z_3^2 - 16\delta^2(28 + 3\delta^2)z_3^3 \\
&\quad + 16(20 + 7\delta^2)z_3^4 - 128z_3^5 \left. \right] (2z_3 - \delta^2) \sqrt{z_3^2 - \delta^2} \\
&\quad - \left[ \delta^4(4 - \delta^2)(4 + \delta^2)(4 + 7\delta^2) - 32\delta^4(1 - \delta^2)(4 + 3\delta^2)z_3 \right. \\
&\quad - 8\delta^2(16 + 40\delta^2 + 57\delta^4 + \delta^6)z_3^2 + 16\delta^2(8 + 58\delta^2 + 3\delta^4)z_3^3 \\
&\quad \left. \left. + 16(16 - 32\delta^2 - 5\delta^4)z_3^4 \right] (4z_3 - 4 - \delta^2) \ln \frac{2z_3 - \delta^2 + 2\sqrt{z_3^2 - \delta^2}}{2z_3 - \delta^2 - 2\sqrt{z_3^2 - \delta^2}} \right\} \times \frac{1}{S_{\text{gluon}}(z_3)} \tag{A1b}
\end{aligned}$$

$e^+e^- \rightarrow Q\bar{Q}[^3S_1^{(1)}] + Q + \bar{Q}$  mode:

$$\begin{aligned}
S_{\text{quark}}(z_3) &= \frac{\pi}{3888} \frac{(\alpha_s \alpha_{EM} \mathcal{Q}_Q)^2}{\delta^3 E^5} \frac{\langle 0 | \mathcal{O}_1^{\psi Q}({}^3S_1) | 0 \rangle}{z_3^3 (z_3 - 2)^6 (z_3^2 - \delta^2)} \\
&\times \left\{ 4z_3 \sqrt{\frac{(1-z_3)(z_3^2 - \delta^2)}{4 + \delta^2 - 4z_3}} \left[ -32\delta^4(4 + \delta^2)(48 + 22\delta^2 + 3\delta^4) \right. \right. \\
&\quad + 32\delta^4(768 + 400\delta^2 + 66\delta^4 + 3\delta^6)z_3 \\
&\quad - 16\delta^2(384 + 1920\delta^2 + 556\delta^4 + 29\delta^6 - 2\delta^8)z_3^2 \\
&\quad + 8\delta^2(1792 + 128\delta^2 - 568\delta^4 - 80\delta^6 - \delta^8)z_3^3 \\
&\quad + 2(2048 - 11008\delta^2 + 10752\delta^4 + 3176\delta^6 + 98\delta^8 + 3\delta^{10})z_3^4 \\
&\quad - 4(4096 - 7808\delta^2 + 3424\delta^4 + 600\delta^6 + 17\delta^8)z_3^5 \\
&\quad + (38912 - 20608\delta^2 + 4544\delta^4 + 508\delta^6 - 3\delta^8)z_3^6 \\
&\quad - 4(13312 - 800\delta^2 + 120\delta^4 - 3\delta^6)z_3^7 + 8(4512 - 20\delta^2 - 15\delta^4)z_3^8 \\
&\quad \left. - 32(336 - \delta^2)z_3^9 + 1280z_3^{10} \right] \\
&\quad - \left[ 8\delta^4(48 + 22\delta^2 + 3\delta^4) - 32\delta^4(24 + 5\delta^2)z_3 \right. \\
&\quad \left. - 2\delta^2(448 + 16\delta^2 + 8\delta^4 - 3\delta^6)z_3^2 + 16\delta^2(56 - 10\delta^2 - 5\delta^4)z_3^3 \right. \\
&\quad \left. + \delta^2(1152 + 272\delta^2 - 3\delta^4)z_3^4 + 8(32 - 92\delta^2 + 5\delta^4)z_3^5 \right. \\
&\quad \left. - 56(16 + \delta^2)z_3^6 + 512z_3^7 \right] \\
&\quad \times \delta^2 (z_3^2 - 2)^4 \ln \frac{z_3 \sqrt{4 + \delta^2 - 4z_3} + 2\sqrt{(1-z_3)(z_3^2 - \delta^2)}}{z_3 \sqrt{4 + \delta^2 - 4z_3} - 2\sqrt{(1-z_3)(z_3^2 - \delta^2)}} \Big\} \tag{A2a}
\end{aligned}$$

$$\begin{aligned}
\alpha_{\text{quark}}(z_3) &= \frac{\pi}{3888} \frac{(\alpha_s \alpha_{EM} \mathcal{Q}_Q)^2}{\delta^3 E^5} \frac{\langle 0 | \mathcal{O}_1^{\psi Q}({}^3S_1) | 0 \rangle}{z_3^3 (z_3 - 2)^6 (z_3^2 - \delta^2)} \\
&\times \left\{ 4z_3 \sqrt{\frac{(1-z_3)(z_3^2 - \delta^2)}{4 + \delta^2 - 4z_3}} \left[ 32\delta^4(4 + \delta^2)(16 + 2\delta^2 + 3\delta^4) \right. \right. \\
&\quad - 32\delta^4(256 + 48\delta^2 + 22\delta^4 + 3\delta^6)z_3 \\
&\quad + 16\delta^2(1152 + 1024\delta^2 - 140\delta^4 - 53\delta^6 - 2\delta^8)z_3^2 \\
&\quad - 8\delta^2(5376 + 128\delta^2 - 1576\delta^4 - 240\delta^6 - \delta^8)z_3^3 \\
&\quad + 2(2048 - 768\delta^2 - 19968\delta^4 - 6968\delta^6 - 350\delta^8 - 3\delta^{10})z_3^4 \\
&\quad \left. - 4(4096 - 20096\delta^2 - 11168\delta^4 - 1208\delta^6 - 43\delta^8)z_3^5 \right. \\
&\quad \left. - 32(336 - \delta^2)z_3^9 + 1280z_3^{10} \right] \\
&\quad \times \delta^2 (z_3^2 - 2)^4 \ln \frac{z_3 \sqrt{4 + \delta^2 - 4z_3} + 2\sqrt{(1-z_3)(z_3^2 - \delta^2)}}{z_3 \sqrt{4 + \delta^2 - 4z_3} - 2\sqrt{(1-z_3)(z_3^2 - \delta^2)}} \Big\}
\end{aligned}$$

$$\begin{aligned}
& + (38912 - 75392\delta^2 - 16960\delta^4 - 996\delta^6 - 3\delta^8)z_3^6 \\
& - 4(13312 - 6304\delta^2 - 872\delta^4 - 3\delta^6)z_3^7 + 8(4512 - 500\delta^2 - 15\delta^4)z_3^8 \\
& - 32(336 - \delta^2)z_3^9 + 1280z_3^{10} \tag{A2b} \\
& + \left[ 8\delta^4(16 + 2\delta^2 + 3\delta^4) - 32\delta^4(8 - \delta^2)z_3 \right. \\
& - 2\delta^2(320 - 272\delta^2 + 64\delta^4 - 3\delta^6)z_3^2 + 16\delta^2(40 - 54\delta^2 - 5\delta^4)z_3^3 \\
& - (1024 - 720\delta^4 - 3\delta^6)z_3^4 + 8(96 - 36\delta^2 - 5\delta^4)z_3^5 \\
& \left. + 8(80 + 7\delta^2)z_3^6 - 512z_3^7 \right] \\
& \times \delta^2(z_3^2 - 2)^4 \ln \left. \frac{z_3 \sqrt{4 + \delta^2 - 4z_3} + 2\sqrt{(1 - z_3)(z_3^2 - \delta^2)}}{z_3 \sqrt{4 + \delta^2 - 4z_3} - 2\sqrt{(1 - z_3)(z_3^2 - \delta^2)}} \right\} \times \frac{1}{S_{\text{quark}}(z_3)}
\end{aligned}$$

## REFERENCES

- [1] C.H. Chang, Nucl. Phys. **B172** 425 (1980).
- [2] E.L. Berger and D. Jones, Phys. Rev. **D23** 1521 (1981).
- [3] J. H. Kühn, J. Kaplan and E. G. O. Safiani, Nucl. Phys. **B157** 125 (1979).
- [4] B. Guberina, J.H. Kühn, R.D. Peccei and R. Rückl, Nucl. Phys. **B174** 317 (1980).
- [5] R. Baier and R. Rückl, Z. Phys. C **19** 251 (1983).
- [6] The CDF collaboration, Fermilab-Conf-94/136-E (1994), unpublished.
- [7] The CDF collaboration, Fermilab-conf-95/128-E (1995), unpublished.
- [8] The CDF collaboration, Fermilab-Pub-95/271-E (1995), unpublished.
- [9] G.T. Bodwin, E. Braaten and G.P. Lepage, Phys. Rev. **D51** 1125 (1995).
- [10] E. Braaten and S. Fleming, Phys. Rev. Lett. **74** (1995) 3327.
- [11] M. Cacciari, M. Greco, M.L. Mangano and A. Petrelli, Phys. Lett. **B356** 553 (1995).
- [12] P. Cho and A.K. Leibovich, Phys. Rev. **D53** 150 (1996).
- [13] P. Cho and A.K. Leibovich, Caltech preprint CALT-68-2026 (hep-ph/9511315).
- [14] E. Braaten and Y.-Q. Chen, Phys. Rev. Lett. **76** 730 (1996).
- [15] J.H. Kühn and H. Schneider, Phys. Rev. **D24** 2996 (1981).
- [16] J.H. Kühn and H. Schneider, Z. Phys. **C11** 253 (1981).
- [17] V.M. Driesen, J.H. Kühn and E. Mirkes, Phys. Rev. **D49** 3197 (1994).
- [18] L. Clavelli, Phys. Rev. **D26** 1610 (1982).
- [19] E. Braaten, K. Cheung and T.C. Yuan, Phys. Rev. **D48** 4230 (1993).
- [20] The CLEO Collaboration, Phys. Rev. **D50** 43 (1994).

[21] The CLEO Collaboration, Phys. Rev. **D52** 2661 (1995).

[22] A. Wolf, Private Communication.